

CanopyShotNoise – An individual-based tree canopy modelling framework for projecting remote-sensing data and ecological sensitivity analysis

Arne Pommerening, Rachel Gaulton, Paul Magdon & Mari Myllymäki

To cite this article: Arne Pommerening, Rachel Gaulton, Paul Magdon & Mari Myllymäki (2021) *CanopyShotNoise* – An individual-based tree canopy modelling framework for projecting remote-sensing data and ecological sensitivity analysis, *International Journal of Remote Sensing*, 42:18, 6837-6865, DOI: [10.1080/01431161.2021.1944695](https://doi.org/10.1080/01431161.2021.1944695)

To link to this article: <https://doi.org/10.1080/01431161.2021.1944695>



© 2021 The Author(s). Published by Informa UK Limited, trading as Taylor & Francis Group.



Published online: 27 Jul 2021.



Submit your article to this journal [↗](#)



Article views: 262



View related articles [↗](#)



View Crossmark data [↗](#)

CanopyShotNoise – An individual-based tree canopy modelling framework for projecting remote-sensing data and ecological sensitivity analysis

Arne Pommerening^a, Rachel Gaulton^b, Paul Magdon^c and Mari Myllymäki^d

^aFaculty of Forest Sciences, Department of Forest Ecology and Management, Swedish University of Agricultural Sciences SLU, Umeå, Sweden; ^bSchool of Natural and Environmental Sciences, Newcastle University, Newcastle upon Tyne, UK; ^cFaculty of Forest Sciences and Forest Ecology, Forest Inventory and Remote Sensing, University of Göttingen, Göttingen, Germany; ^dNatural Resources Institute Finland (Luke), Bioeconomy and Environment Unit, Helsinki, Finland

ABSTRACT

Very few spatially explicit tree models have so far been constructed with a view to project remote-sensing data directly. To fill this gap, we introduced the prototype of the *CanopyShotNoise* model, an individual-based model specifically designed for projecting airborne laser scanning (ALS) data. Given the nature of ALS data, the model focuses on the dynamics of individual-tree canopies in forest ecosystems, that is, spatial tree interaction and resulting growth, birth and death processes. In this study, *CanopyShotNoise* was used to analyse the long-term effects of the processes *crown plasticity* (C) and *super-organism formation* (S) on spatial tree canopy patterns that are likely to play an important role in ongoing climate change. We designed a replicated computer experiment involving the four scenarios C0S0, C1S0, C0S1 and C1S1 where 0 and 1 imply that the preceding process was switched off and on, respectively. We hypothesized that C and S are antagonistic processes, specifically that C would lead to increasing regularity of tree locations and S would result in clustering. Our simulation results confirmed that in the long run intertree distances decreased and canopy gap size increased when superorganisms were encouraged to form. At the same time, the overlap and packing of tree crowns increased. The long-term effect of crown plasticity increased the regularity of tree locations; however, this effect was much weaker than that of superorganism formation. As a result, gap patterns remained more or less unaffected by crown plasticity. In scenario C1S1, both processes interestingly interacted in such a way that crown plasticity even increased the effect of superorganism formation. Our simulation results are likely to prove helpful in recognizing patterns of facilitation with ongoing climate change.

ARTICLE HISTORY

Received 13 February 2021
Accepted 28 April 2021

1. Introduction

Canopies are the photosynthetically active macro-organs of trees. The assimilating leaves are usually organized in large clusters, which are often referred to as crowns or canopy.

CONTACT Arne Pommerening  arne.pommerening@slu.se  Swedish University of Agricultural Sciences SLU, Faculty of Forest Sciences, Department of Forest Ecology and Management, Skogsmarksgränd 17, SE-901 83 Umeå, Sweden.

© 2021 The Author(s). Published by Informa UK Limited, trading as Taylor & Francis Group.
This is an Open Access article distributed under the terms of the Creative Commons Attribution-NonCommercial-NoDerivatives License (<http://creativecommons.org/licenses/by-nc-nd/4.0/>), which permits non-commercial re-use, distribution, and reproduction in any medium, provided the original work is properly cited, and is not altered, transformed, or built upon in any way.

Growing large stems and pushing crowns upwards has been a key evolutionary strategy that trees have adopted in contrast to other plants (Falster and Westoby 2003). Understanding gap dynamics and associated light environments, nutrient and water cycling throughout the vertical canopy is, therefore, key to studying forest ecosystem processes and patterns. Ongoing climate change has been found to affect forest canopies and, therefore, models focusing on tree crown patterns will contribute to a better understanding of climate-induced effects and their distribution in space (Nakamura et al. 2017; Senf et al. 2018).

Recent research has also highlighted that trees are less sessile than we often believe (Purves, Lichstein, and Pacala 2007; Schröter, Härdtle, and von Oheimb 2012; Uria-Diez and Pommerening 2017; Vovides et al. 2018). Particularly in forest stands, they often adjust the shape and locations of their crowns in an attempt to optimize the assimilation gain. Whilst in the past, spatially explicit research in forest ecology has almost exclusively focused on stem-centre coordinates, new research appears to suggest that important ecological signals may have been missed (García 2014): Where in former times – when using stem-centre coordinates – it was, for example, concluded that observed tree-location patterns were close to complete spatial randomness, inhibition processes had in fact already started leading to regularly dispersed trees or overdispersion (Gavrikov, Grabarnik, and Stoyan 1993). The definition of stem-centre coordinates as traditional spatial reference of trees has originally stemmed from practice in forest inventory (Gregoire and Valentine 2008). Here, a definition was necessary to decide which trees were included in inventory plots and stem-centre coordinates were taken as convenient reference to meet this requirement (Pommerening and Sánchez-Meador 2018). The same spatial reference was later adopted in spatial ecology. However, these coordinates are conservative, since tree stems can hardly move, unless soil movements (e.g. landslides) or excessive mortality cause spatial tree patterns to change considerably. By contrast, tree crowns are very dynamic and crown-based coordinates can considerably deviate from stem-centre coordinates, a phenomenon which is often termed *crown plasticity*. Some crown movements are caused by environmental conditions (Vovides et al. 2018) such as wind and snow or by topography (slopes); however, to a large extent they are due to the struggle for light and due to physical forces between the tree crowns. Over the last two decades, average differences between stem-centre and crown-based coordinates of 2–4 m have been reported (Gavrikov, Grabarnik, and Stoyan 1993; García 2014; Pommerening and Uria-Diez 2017; Schröter, Härdtle, and von Oheimb; Vovides et al. 2018). Such differences can considerably influence the spatial pattern of forests so that the results obtained from using only stem-centre coordinates in the spatial analysis can lead to inadequate conclusions.

Apart from crown plasticity, there is another important process influencing the spatial patterns of tree locations in forest stands. Research in belowground forest ecology has suggested that trees often form root connections through mycorrhiza networks and through simple grafting (Gorzalak et al. 2015). This can potentially lead to a physiological connection or even union that could be termed ‘superorganism’. The formation of superorganisms is an extreme form of mutualism with a benefit for all trees involved (Perry, Oren, and Hart 2008). Mutualism is a form of facilitation that according to the stress-gradient hypothesis is said to increase when biotic and abiotic stress increases (Bertness and Callaway 1994). The formation of superorganisms is supported by the

frequent perception of two or more individuals sharing a common tree crown rather than shying away from each other (Till-Bottraud, Fajardo, and Rioux 2012). How crown plasticity and the formation of superorganisms interact is largely uncertain and dynamic tree models such as *CanopyShotNoise* can contribute to a better understanding of how these processes potentially influence spatial tree patterns of forests. For developing and applying such a dynamic model, spatially explicit time series involving tree locations and crown shapes are required.

Remote-sensing methods have the potential to provide such data efficiently for large areas. In particular, Airborne Laser Scanners (ALS) with their ability to penetrate the forest canopy have been successfully used to map individual-tree locations and crown shapes (Xiao et al. 2019) and in many cases even time series based on repeated airborne surveys are available that span over a decade or more (Bolton et al. 2018). For example, a multi-year time series between 2006 and 2014 including four airborne LiDAR (**L**ight **D**etection and **R**anging) acquisitions is available for Queen Elizabeth II Forest Park, Scotland, UK. Recently such data have also been made available from drone-based photogrammetry and laser scanning (Iglhaut et al. 2019), which can be acquired at high temporal frequencies, albeit over small spatial extents.

This availability of high-resolution point cloud data from forest canopies has given rise to a wide range of applications in forest and ecological modelling, which largely fall into two main groups i) the *area-based approach* (ABA) breaking down the total area of a forest stand into regular grid cells and linking point cloud metrics of the cells with target variables using parametric and non-parametric models, and ii) the *individual-tree detection* (ITD) approach segmenting individual tree crowns in the point cloud for which a number of metrics (e.g. crown area, tree height, crown volume) are calculated as shown in Figure 1. ABA has been widely applied in forest ecology (see, for example, Heidrich et al. 2020; Jung et al. 2012; Müller et al. 2009) to estimate forest stand characteristics (see Shang et al. 2017; Zhang et al. 2019) and is often employed in the context of national forest inventories (Næsset et al. 2014; Nilsson et al. 2017; Magnussen, Nord-Larsen, and Riis-Nielsen 2018; White et al. 2013). The method is also applied in forest growth and yield modelling where first stand characteristics such as total height, species, basal area and mean diameters are predicted from ALS metrics which then provide inputs to growth models that were originally not designed for remote-sensing data (e.g. Falkowski et al. 2010; Marczak et al. 2020; Tompalski et al. 2018). With the advent of enhanced methods for single tree detection (Reitberger et al. 2014; Li et al. 2012), the number of studies that utilize individual tree information is increasing. However, there are only a few studies that link individual-tree crown attributes with models (Packalen, Pukkala, and Pascual 2020; Pascual 2021). Again very few of these directly employ ALS-derived tree crown shapes to model forest development (Ma et al. 2018; Pont et al. 2021; Versace et al. 2019). To the best of our knowledge, the potential for the use of ALS-derived individual-tree crown or canopy metrics in dynamic forest models has been little explored.

Given the increasing importance of remote sensing in forest ecology and management, it is a sensible idea to directly link individual-based tree models with single-tree traits derived from remote sensing to avoid the detour of data transformation and the associated potential loss of information in the process. This way we gain new insights on spatial pattern forming processes based on real-world observational data.

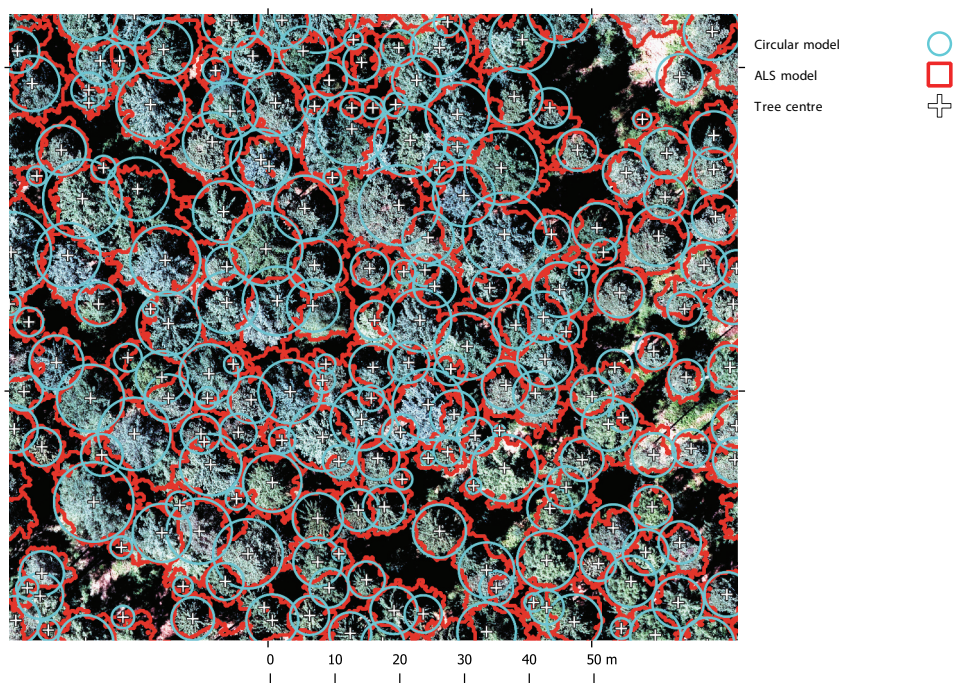


Figure 1. Example of individual-tree detection from a mixed-species forest stand including Norway spruce (*Picea abies* (L.) H. KARST.) and Scots pine (*Pinus sylvestris* L.) trees in 2018 at Gartow in northern Germany. The red lines represent the irregular crown boundaries that were detected by the segmentation algorithm. The cyan lines represent circular crowns with the same areas and centre coordinates. The background shows a true-colour digital ortho-mosaic with a spatial resolution of 5 cm.

The objectives of this study are (1) to propose *CanopyShotNoise*, a spatially explicit individual-based forest model, that can be parameterized based on ALS-derived single-tree information and project crown sizes and locations and (2) to illustrate the model's capabilities for exploring the consequences of crown plasticity and of the formation of superorganisms compared to scenarios without these processes. We hypothesized that in the long term crown plasticity would lead to increasing regularity of tree locations, also termed overdispersal, and that the formation of superorganisms would result in clustering or underdispersal. This would imply that crown plasticity would leave small gaps in the forest stand canopy whilst with superorganism formation gaps would be markedly larger.

2. Methods

2.1. Description of the model framework

2.1.1. Interaction field and crown-diameter growth

The spatio-temporal evolution of plant patterns can be modelled accurately by spatially explicit individual-based models (IBM). This concept has origins in different fields of natural sciences including the ecological field theory (Wu et al. 1985; Miina and Pukkala 2002), shot-noise fields in physics (Baccelli and Blaszczyzyn 2001), individual-based modelling (Snyder and Chesson 2004; Adams et al. 2011), competition kernels (Vogt,

Murrell, and Stoll 2010) and growth-interaction models (Renshaw and Särkkä 2001; Särkkä and Renshaw 2006; Cronie, Nyström, and Yu 2013; Häbel, Myllymäki, and Pommerening 2019). In these models, every plant of a given community emits a signal, which is largest at or near the location of a plant and decreases with increasing distance from that plant. These local signals are described by probability density functions, the so-called kernel functions. They express the contribution of a plant to the interaction field. The signals can be aggregated additively or multiplicatively at any point in the observation window leading to interaction fields, which are characteristic of these model approaches. The interaction field obtained from aggregating or superimposing individual plant signals largely drives the ecological processes of the model such as interaction, growth, survival and birth.

The starting point for our new modelling framework was the *TreeShotNoise* model documented in Pommerening, LeMay, and Stoyan (2011), Pommerening and Särkkä (2013), Häbel, Myllymäki, and Pommerening (2019) and Pommerening and Grabarnik (2019, Chapter 5.2.10). Since the new modelling framework has a different focus and is based on different principles, we refer to the new model as *CanopyShotNoise* throughout this text for better discrimination. The main mark, that is, the key tree variable, modelled and projected in *CanopyShotNoise* is tree crown diameter, w , thus resulting in simplified, circular crown projection areas. In future model applications, it is naturally also possible to consider irregular crown shapes, since the necessary information is provided by ALS remote sensing. The general concept of the model can be adapted to any vegetation that forms canopy clusters such as trees and shrubs. We included total tree height as a secondary mark, as this information is often useful in follow-on analyses and tree heights can be measured with high precision at low cost using ALS data.

In the model, we considered relative growth rates (RGR) of crown diameters as response variables. These are estimated for updating crown diameters and total heights. In our approach, mean periodic RGRs are computed as

$$\bar{r}_{i,t} = \frac{\log_e w_{i,t} - \log_e w_{i,t-\Delta t}}{\Delta t} \quad (1)$$

following conventions in general plant science (Pommerening and Grabarnik 2019, 263). $w_{i,t}$ denotes crown diameter of tree i at current time t and $w_{i,t-\Delta t}$ is crown diameter measured at time $t - \Delta t$ in the past. In the case of annual time steps as used in *CanopyShotNoise*, Equation (1) simplifies because $\Delta t = 1$. In our model, we considered a transformation of RGR, the *growth multiplier*, $M_{i,t}$, which is obtained from Equation (1) by calculating $M_{i,t} = e^{\bar{r}_{i,t}}$, assuming again annual time steps (Pommerening and Grabarnik 2019, 264). The growth multiplier is a function of relative growth rate and defined as the ratio of a particular plant size characteristic at different times, that is, in our case $M_{i,t} = \frac{w_{i,t}}{w_{i,t-1}}$ for all times t (Wenk 1972). Circumstances where $M_{i,t} > 1$ indicate growth, the condition $M_{i,t} = 1$ occurs where there is no growth and with $M_{i,t} < 1$ the corresponding plant size characteristic shrinks. All these three conditions apply in *CanopyShotNoise*. The potential growth multiplier of tree crown diameter was modelled using a power function (Pommerening and Grabarnik 2019, 287; Figure 2).

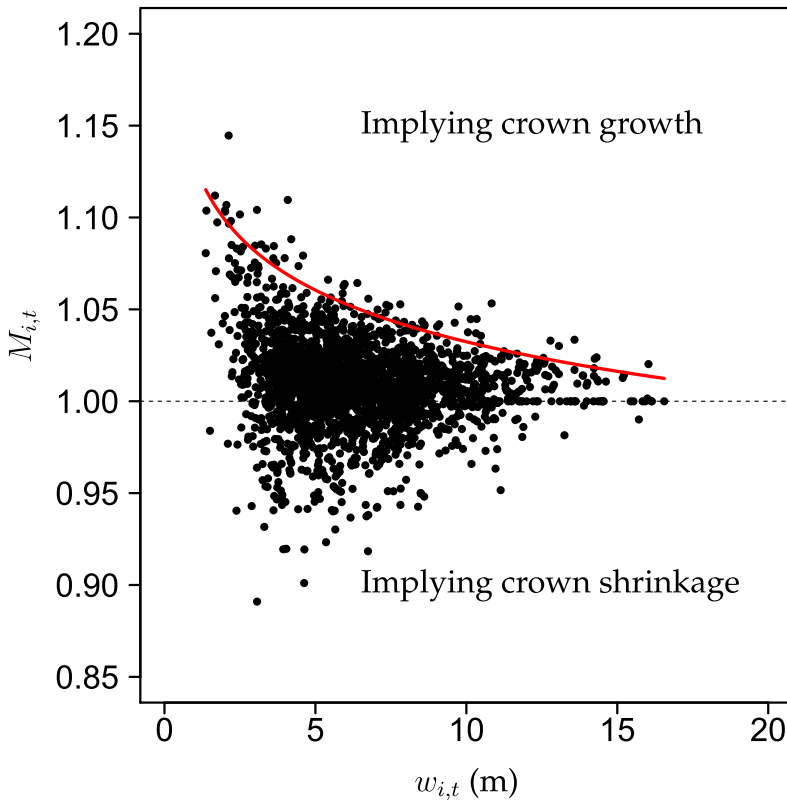


Figure 2. Annual growth multiplier $M_{i,t}$ pooled from a total of 17 *F. sylvatica* plots in the Swiss forest regions of Aarburg, Concise, Embrach, Zofingen and Zollikon. The red curve represents potential tree crown growth multiplier using Equation (2) and quantile regression (Cade and Noon 2003) with $\tau = 0.975$.

$$M_{i,t}^{\text{pot}} = k \times w_{i,t}^{-q} \quad (2)$$

The power function of Equation (2) is a function of the current size of the tree crown, $w_{i,t}$. $M_{i,t}^{\text{pot}}$ is the potential growth multiplier of the tree-crown diameter and k and q are the model parameters to be estimated from mean periodic RGR measured in repeated surveys, see Equation (1). In future versions of the model it would also be possible to estimate $M_{i,t}^{\text{pot}}$ from tree physiology parameters and environmental covariates.

A key element of the *CanopyShotNoise* model is the aforementioned shot-noise interaction field. This interaction field is the result of additively aggregated interaction signals. Following the shot-noise methodology outlined in Häbel, Myllymäki, and Pommerening (2019), an interaction function $H_{i,t}$ (Equation 4) aggregates interaction signals emitted by each tree j at the location of subject tree i . The interaction signals are modelled using a Gaussian kernel density function that depends on the distance from the subject tree but also on its mark (Figure 3(a), Equation 3). In contrast to the Gaussian kernel used in *TreeShotNoise* (Häbel, Myllymäki, and Pommerening 2019), $w_{j,t}^a$, the maximum value of the interaction signal, is continued throughout the extent of the circular crown projection

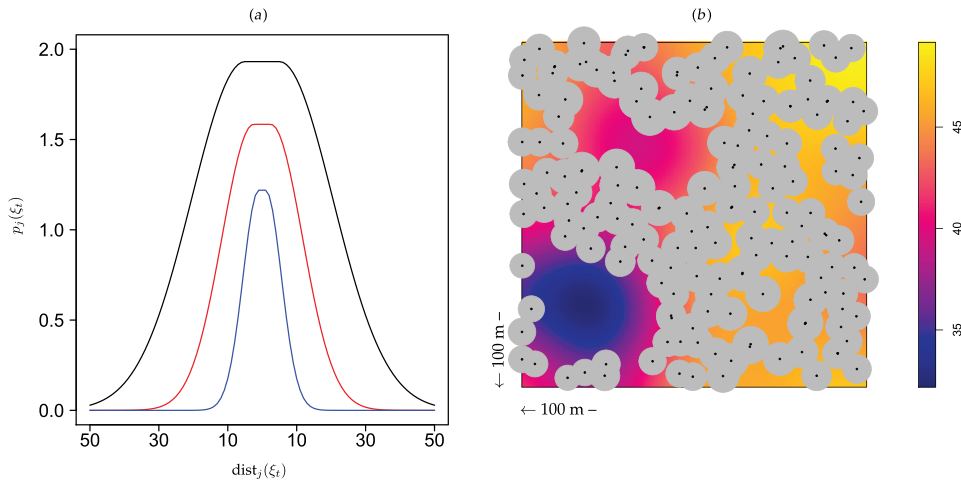


Figure 3. (a): Gaussian kernel and local effect according to Equation (3) with $\alpha = 0.24782$, $\beta = 1.60597$ and $\delta = 0.07471$ for *F. sylvatica* trees with a crown diameter $w_{j,t}$ of 2 (blue), 5 (red) and 10 m (black). The unit of distance $\text{dist}_j(\xi_t)$ is metres. (b): shot-noise field of a model simulation of *F. sylvatica* in a 100×100 m observation window after 34 years. The union of filled grey circles represent tree crowns and the black dots denote the tree locations. The colours indicate the different intensities of the shot-noise field. The largest field values are indicated by yellow and orange colours, the lowest by blue colours.

area of a given tree and only decreases beyond the boundaries defined by the crown radius (Berger and Hildenbrandt 2000):

$$p_{j,t}(\xi_{i,t}) = \begin{cases} w_{j,t}^\alpha, & \text{for } 0 \leq \text{dist}_j(\xi_{i,t}) < \frac{w_{j,t}}{2} \\ w_{j,t}^\alpha \times e^{-\left\{ \frac{\delta \times (\text{dist}_j(\xi_{i,t}) - \frac{w_{j,t}}{2})^2}{w_{j,t}^\beta} \right\}}, & \text{otherwise} \end{cases} \quad (3)$$

The Gaussian kernel function has three model parameters α , β and δ . Increasing the value of α increases the strength of the interaction signal, whilst β and δ affect the range of the interaction signal (Pommerening, LeMay, and Stoyan 2011). At any location ξ_t in the observation window, the sum $H_t(\xi_t) = \sum p_{j,t}(\xi_t)$ defines the shot-noise field at time t (Figure 3(b)). In *CanopyShotNoise*, the tree locations are essentially crown-centre coordinates and can potentially change from year to year. The interaction function $H_{i,t}$ describing the interaction between trees j and tree i is the sum of local interaction effects $p_{j,t}(\xi_{i,t})$ divided by the interaction signal value of the subject tree at its own location:

$$H_{i,t} = \sum_{j \neq i} \frac{p_{j,t}(\xi_{i,t})}{w_{i,t}^\alpha} \quad (4)$$

Dividing by $w_{i,t}^\alpha$ scales, the strength of interaction according to the crown size of subject tree i . Finally, following Häbel, Myllymäki, and Pommerening (2019), interaction is standardized as in Equation (5).

$$H_{i,t}^* = 1 - e^{-\frac{\nu}{H_{i,t}}} \quad (5)$$

In Equation (5), ν is another model parameter. The estimated growth multiplier of the tree crown mark can now be simply calculated as

$$M_{i,t} = M_{i,t}^{\text{pot}} \times H_{i,t}^* \quad (6)$$

Crown diameter $w_{i,t-1}$ from year $t - 1$ is then updated by multiplication with $M_{i,t}$:

$$w_i = M_{i,t} \times w_{i,t-1} \quad (7)$$

Finally total tree height $h_{i,t}$ of tree i at time t is calculated from crown diameter through the *crown spread ratio*, that is, $\frac{w_{i,t}}{h_{i,t}}$ and the Michaelis-Menten saturation model (Michaelis and Menten 1913; Bolker 2008, 77ff.):

$$h_{i,t} = \frac{b + w_{i,t}}{a}. \quad (8)$$

Equation (8) was motivated by the relationship between total tree height and crown diameter found in the Swiss *F. sylvatica* data, see Section 2.2. $h_{i,t}$ played a minor role in this study, but can be important information in other contexts.

2.1.2. Mortality

The mortality model was adopted from *TreeShotNoise* as described in Häbel, Myllymäki, and Pommerening (2019) and Pommerening and Grabarnik (2019, Chapter 5.2.10). Mortality here depends on the five-year growth performance that in turn is determined by a combination of potential crown growth and interaction. The aforementioned crown growth multiplier $M_{i,t}$ is interpreted as an indicator of growth performance. For a given tree i , a memory function aggregates and updates the growth multipliers $M_{i,t}$ of the last five years:

$$M_{i,t}^{(5)} = M_{i,t} \times M_{i,t-1} \times \dots \times M_{i,t-4} \quad (9)$$

If the simulated five-year growth multiplier falls short of a critical value, the tree dies. This critical value $M_{i,t}^{(5,\text{crit})}$ is dependent on crown size and is calculated from the power function $M_{i,t}^{(5,\text{crit})}(w_{i,t}) = c_t \times w_{i,t}^{-d}$, where c and d are model parameters. The power function takes the dynamics of relative growth rates into account, specifically the size influence leading to a trend where smaller plants typically tend to have large and larger plants tend to have small RGRs (Pommerening and Muszta 2016; Pommerening and Grabarnik 2019, Chapter 6). In *CanopyShotNoise*, model parameter c_t is additionally made dependent on *canopy cover fraction* v_t , that is, on the proportion of forest stand area covered by tree crowns (Pretzsch 2009, 267):

$$c_t = \frac{c_0 \times v_t}{c_1 + v_t}. \quad (10)$$

The canopy cover fraction v_t is the grey area of united crowns in Figure 3(b) relative to the total area of the observation window. In Equation (10), again the Michaelis–Menten saturation model is used to describe model parameter c_t . The more canopy density increases the larger $M_{i,t}^{(5,\text{crit})}$, leading to increased mortality. However, the saturation model ensures that

mortality rates do not continue to increase exponentially with increasing canopy density. With decreasing canopy caused by mortality $M_{i,t}^{(5,crit)}$ decreases as well. This model component supports the fact that in forest ecosystems light availability typically decreases as canopy cover fraction increases and at the same time mortality increases.

2.1.3. Birth processes

The birth process of *CanopyShotNoise* was modelled as an immigration-death process, since detailed data on seed dispersal and germination are often unavailable. The term immigration in our model framework therefore relates to tree saplings. In our immigration-death process, individuals arrive in observation window W at random points in time according to a Poisson process on $[0, T]$ with annual intensity $\lambda_B > 0$ and T is the total simulation time (see Särkkä and Renshaw 2006). A given simulation year is considered an arrival year of immigrants, if a uniformly distributed random number between 0 and 1 is less than an exponentially distributed random number drawn for that particular simulation year with intensity λ_B . In the arrival years t_1, \dots, t_{N_B} , each existing parent tree contributes $N_{i,t}^{(B)} = f \times \pi \times \left(\frac{w_{i,t}}{2}\right)^2$ immigrants, where f is the birth rate per m^2 (Adams et al. 2011; Nanos, Larson, and Millerón 2010). The $N_{i,t}^{(B)}$ trees are assigned to random, uniformly distributed locations ξ in W (Cronie, Nyström, and Yu 2013). Crown diameters are assigned to these immigrants by an exponential marking model (Ho and Stoyan 2008; Myllymäki and Penttinen 2009) similar to Equation (13) with the difference that crown diameter is dependent not on local point density $\Lambda(\xi_i)$ but on the shot-noise field, more precisely on

$$H_k = \sum_{j \neq i} p_j(\xi_k) \quad (11)$$

where ξ_k are the locations of the tree immigrants and $p_j(\xi_k)$ are the unweighted local effects from Equation (3). The resulting interaction values are a function of local canopy density. The total tree heights of the immigrants are again obtained from crown diameters based on Equation (8).

Finally, the new immigrants are thinned by the shot-noise field. The thinning mimics immediate seedling death shortly after germination, hence the term immigration-death process. For this, Equation (11) is again calculated for all immigrants and the H_k values are standardized based on both established trees and new immigrant trees through the well-known equation $H_k^* = \frac{H_{k,t} - \min(H_{k,t})}{\max(H_{k,t}) - \min(H_{k,t})}$. Immigrant trees die instantly, if H_k^* is larger than a random number drawn from a uniform distribution between 0 and 1. The values of $M_{i,t}, M_{i,t-1}, \dots, M_{i,t-4}$ of the survivors are initialized with a value of 1.5 each and the general mortality model as described in Section 2.1.2 starts to affect the immigrants along with all other trees in the following year.

2.1.4. Crown plasticity

A particular feature of *CanopyShotNoise* is to allow tree crowns to change and optimize their crown locations according to the shot-noise field (Figure 3(b)). The shot-noise field is essentially a map of local interaction intensity. As mentioned in Section 1, crown plasticity is quite common in nature (Uria-Diez and Pommerening 2017; Schröter, Härdtle, and von

Oheimb 2012; Vovides et al. 2018) and somewhat questions the use of stem-centre coordinates that usually form the basis of spatial tree analyses (García 2014). We simulated crown plasticity in such a way that every year each tree has 100 attempts to improve its competitive situation by moving to a new location within a radius R around its current location. That location is approved as new tree location where H_k (Equation 11) is smallest. Index k here denotes the trial locations within circles defined by R . If no location with a smaller H_k can be found, the given tree remains at its current location. This crown plasticity process was simulated sequentially, that is, one tree at a time attempted to find a more suitable tree location until the whole tree list was processed.

2.1.5. Superorganisms

In *CanopyShotNoise*, it is also possible that trees at close proximity form a superorganism. Although such trees in the model retain their individual crowns, circular crown projection areas and coordinates as well as the opportunity to move separately, a group of trees acting as one superorganism ceases to compete with each other for resources. This gives trees that are part of a superorganism an advantage over those that continue to be individual, solitary trees. The cumulative growth rates of trees forming a superorganism are also less likely to fall below the mortality threshold $M_{i,t}^{(S,crit)}$, see Section 2.1.2.

In our model, the formation of superorganisms is based on crown overlap. Crown overlap exists, if the sum of crown radii of a pair of trees is larger than the distance between them (Pommerening and Grabarnik 2019, 227, see Figure 4).

We turned this fact into a rule for the formation of superorganisms. Not considering time t for the ease of reading, two trees form a superorganism, if

$$\frac{w_i}{2} + \frac{w_j}{2} > \text{dist}_j(\xi_i). \quad (12)$$

This means that the two trees satisfying Equation (12) cease to contribute to each other's competition load in Equation (4). The rule described in Equation (12) implies that the ratio of crown-radius sum and distance must be larger than a superorganism characteristic S , which is another model parameter. For two tree crowns to overlap, the condition $S > 1$

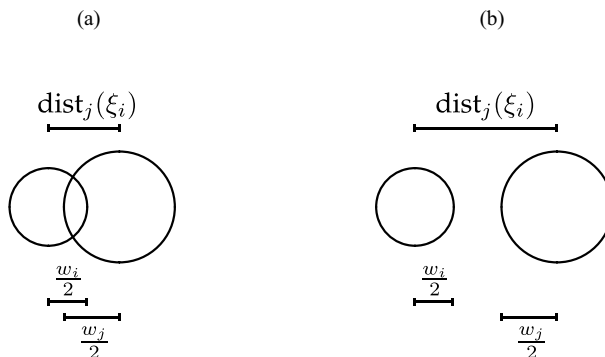


Figure 4. Principle of crown overlap (without considering time t): tree crowns overlap (a), if $\frac{w_i}{2} + \frac{w_j}{2} > \text{dist}_j(\xi_i)$, otherwise they do not (b), where w is tree crown diameter. The two crowns in each example are indicated by open circles. Modified from Pommerening and Grabarnik (2019, 227).

must be satisfied. The larger S the more crown overlap is required to ‘formally’ recognize trees as superorganisms. The rule also allows for multiple neighbours j to form a superorganism with the same tree i .

In simulations, the superorganism rule often leads to small clusters of 2–4 medium- to large-sized tree crowns and consequently to a more compact packing of tree canopies. Another consequence of the formation of superorganisms is the increased survival of small-canopy trees under the canopy of very large trees, which can often be observed in nature (LeMay, Pommerening, and Marshall 2009).

2.2. Parameter estimation

CanopyShotNoise is a generic model without any particular reference to species or geography. In future applications of the model to specific tree populations and forest ecosystems, the parameterization can entirely be based on remotely sensed data or on a combination of remotely sensed and terrestrially measured data. For deriving suitable shot-noise parameters α, β, δ , a time series of remotely sensed or terrestrially measured data is required.

For illustrating the modelling framework in this paper, the tree crown and height characteristics as well as the shot-noise field were loosely based on the species European beech (*Fagus sylvatica* L.). Spatially explicit terrestrial data were gratefully obtained from the Swiss Federal Institute of Forest, Snow and Landscape Research (WSL). The 5591 spatial tree records (crown radii, total tree heights and tree coordinates) were collected in a total of 17 plots at each of the five sites at Aarburg, Concise, Embrach, Zofingen and Zollikon and were used to establish growth potential parameters and the parameters of the shot-noise field. These time series had 4–9 re-measurements at variable survey intervals with an average of 7 years.

Parameter estimation largely followed Häbel, Myllymäki, and Pommerening (2019) and proceeded in two main steps (see Table 1). Firstly, we estimated the parameters of the

Table 1. Main parameters of the *CrownShotNoise* model, their descriptions and values as used in this study.

Parameter	Description	Value
k	Parameter of the power function modelling potential growth multiplier as a function of crown diameter, Equation (2)	1.1287
q	Parameter of the power function modelling potential growth multiplier as a function of crown diameter, Equation (2)	-0.0387
α	Shot-noise parameter scaling kernel strength (Equation 3)	0.2478
β	Shot-noise parameter scaling kernel range (Equation 3)	1.6060
δ	Shot-noise parameter scaling kernel range (Equation 3)	0.0747
ν	Parameter used in standardizing the interaction function $H_{i,t}^*$ (Equation 5)	96.3815
a	Total tree height estimation parameter (Equation 8)	0.5697
b	Total tree height estimation parameter (Equation 8)	9.1091
c_0	Mortality threshold parameter (Equation 10)	1.0200
c_1	Mortality threshold parameter (Equation 10)	0.0200
d	Mortality threshold parameter	0.0060
λ_B	Annual birth intensity	0.0390
f	Birth rate per square metre crown projection area	0.0900
R	Every year each tree can shift its current location to a new one within a radius of R m.	0.4000
S	To be recognized as part of a superorganism, the sum of a tree's crown radius and that of a neighbour divided by the distance between them must be larger than S (Equation 12).	1.3000

potential growth multiplier of tree crown diameter (Equation 2), k and q , separately from the remainder of the model and directly from the observed data as an upper quantile of the observed mark growth rates applying quantile regression (Koenker and Park 1994; Cade and Noon 2003), where the quantile selected was set to $\tau = 0.975$.

Secondly, the interaction parameters α, β and δ were estimated through nonlinear spatial regression using the growth multiplier of crown diameters as dependent variables. As in Häbel, Myllymäki, and Pommerening (2019), we applied both a nonlinear least-squares and a maximum-likelihood approach for estimating the interaction parameters by initially using the same starting values. Then, we evaluated least-squares loss at the maximum-likelihood location. Finally, we fitted the maximum-likelihood model using the least-squares parameter estimates as starting points. We also checked quantile-quantile plots, homoscedasticity of residuals and the shape of the interaction kernels. The parameter estimates of both methods usually were quite similar. In this estimation process, we applied periodic boundary conditions (Pommerening and Grabarnik 2019, 177) for spatial edge correction.

All other model parameters were freely determined in such a way that the model would simulate continuous forest development without any instances where no trees at all would occur in the observation window at any time (Table 1). Given the objectives of this study, crown plasticity and superorganisms were considered as model inputs in order to study how these processes affect the formation of spatial canopy patterns.

2.3. Model scheduling

CanopyShotNoise operates in discrete, annual time steps and at the beginning of each time step first the mortality rule is applied followed by a removal of all dead trees (Figure 5). Afterwards the interaction term is calculated, which contributes to the annual relative growth rates of the crown diameter mark. The superorganism rule is part of the interaction calculation. In the same way as in the parameter estimation, the interaction

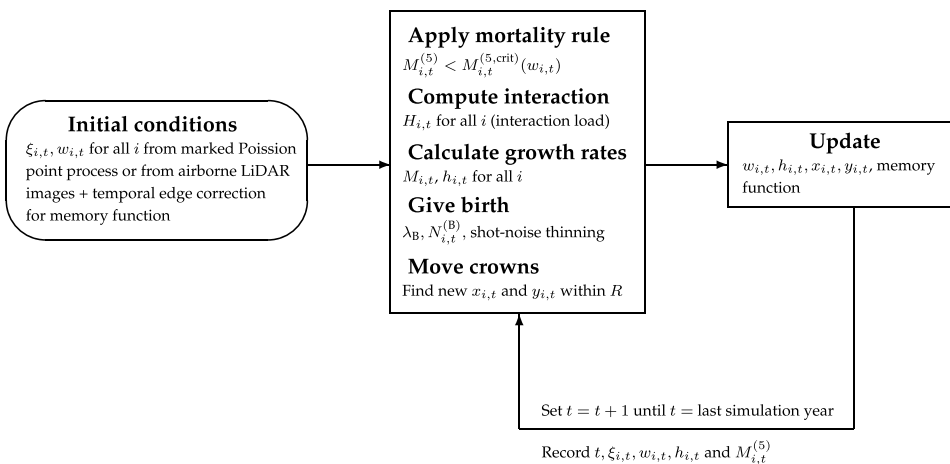


Figure 5. Flowchart of the *CanopyShotNoise* model simulation. The meaning of the symbols is explained in Section 2.1.

term is calculated using periodic boundary conditions (Pommerening and Grabarnik 2019, 177). After calculating interaction and canopy growth, the tree crown diameters and total heights are updated synchronously.

Each model cycle is continued by simulating small immigrant trees, if that particular year is selected as an arrival year. The immigrants surviving the shot-noise thinning are included in the tree population. The model cycle is completed by calculating crown movements and updating the new tree coordinates.

2.4. Model initialization

In future applications of *CanopyShotNoise*, it is possible to initialize the model with an observed crown map obtained from airborne laser scanning. For the experiments performed in this study, the model was initialized with a Poisson point process model with intensity $\lambda = 0.025$ points per m^2 in an observation window with 100 m side lengths mimicking the pattern of a very young forest. Any other point process model and intensity are naturally also possible. In a second step, initial crown diameters were simulated using an exponential marking model (Ho and Stoyan 2008; Myllymäki and Penttinen 2009) that is dependent on local point intensity, that is, the lower local point density the larger are the estimated crown diameters (Equation 13). Conversely, in areas of high local point density, the estimated crown diameters are comparatively small. Local point density was estimated using the spatstat function density (Baddeley, Rubak, and Turner 2016).

$$w(\xi_i) = 12.3 \times e^{-75\Lambda(\xi_i)} \quad (13)$$

Here, ξ_i denotes the location of tree crown i whilst $\Lambda(\xi_i)$ is the local point density at ξ_i . The inspiration for this initialization was taken from the Boolean model of random set statistics (Chiu et al. 2013).

2.5. Experimental model settings and simulations

In this study, we were mainly interested in evaluating the likely influence of crown plasticity and the formation of superorganisms on emerging crown canopy patterns. Therefore, we considered four scenarios

- (1) No crown plasticity + no superorganism formation (scenario: C0S0),
- (2) Crown plasticity + no superorganism formation (scenario: C1S0),
- (3) No crown plasticity + superorganism formation (scenario: C0S1),
- (4) Crown plasticity + superorganism formation (scenario: C1S1).

Scenario 1 (C0S0) can be considered a baseline reference, whilst scenario 4 (C1S1) covers potential interactions of crown plasticity and the formation of superorganisms. Since this was an explorative study with a prototype model, we decided to interpolate between extreme model settings rather than varying the model parameters on a continuous scale, which would lead to many results that are hard to present in a single scientific paper. To gain clear signals, we have, therefore, applied the following model settings: $R = 40$ cm, $S = 1.3$, see Sections 2.1.4 and 2.1.5. The settings allow every tree each year to move away

from its current location within a radius of 40 cm, which is at the upper end of currently available observations of annual shifts (Uria-Diez and Pommerening 2017; Vovides et al. 2018). In a similar way, superorganisms are formed as soon as the sum of crown radii of two trees divided by the distance between their locations exceeds 1.3. In the absence of physiological evidence, this assumption describes situations of small crown overlaps, that is, the formation of superorganisms is strongly encouraged in the simulations.

After initial trial simulations and tests to assess the variability of simulation outcomes, we decided to simulate each of the four scenarios 500 times. Each simulation included a period of 100 years to allow studying the long-term effects of crown plasticity and the formation of superorganisms.

2.6. Summary characteristics

We identified and tested three summary characteristics from spatial statistics that described the differences in simulated tree canopy patterns particularly well.

The *nearest-neighbour distance density function* $d(r) = D'(r)$ gives the density of the nearest-neighbour distance distribution function $D(r)$. In our study, both quantities are based on the distance $\text{dist}(\xi)$ from a tree's coordinates ξ to those of its first nearest neighbour. For clarity, we omitted index t pertaining to the tree locations in the following equations. Illian et al. (2008, 211) give a suitable estimator as

$$\hat{d}(r) = \sum_{\xi} \frac{k_h(\text{dist}(\xi) - r) \frac{\mathbf{1}_{W_{\ominus \text{dist}(\xi)}}(\xi)}{A(W_{\ominus \text{dist}(\xi)})}}{\hat{\lambda}_{\text{nn}}} \quad (14)$$

Here, $\mathbf{1}_{W_{\ominus \text{dist}(\xi)}}(\xi)$ is an indicator function returning the value of 1, if $\text{dist}(\xi)$ is smaller than the shortest distance between ξ and the boundary of observation window W and 0 otherwise. $A(W_{\ominus \text{dist}(\xi)})$ gives reduced areas of the observation window dependent on $\text{dist}(\xi)$. k_h denotes an appropriate kernel function with bandwidth h , in our case the Epanechnikov kernel, see Pommerening and Grabarnik (2019, 152), whilst $\hat{\lambda}_{\text{nn}}$ is a density estimator that computes as

$$\hat{\lambda}_{\text{nn}} = \sum_{\xi, \text{dist}(\xi)} \frac{\mathbf{1}_{W_{\ominus \text{dist}(\xi)}}(\xi)}{A(W_{\ominus \text{dist}(\xi)})} \quad (15)$$

This form of estimator $\hat{d}(r)$ corresponds with the Hanisch edge correction estimator of nearest-neighbour functions (Hanisch 1984).

A complementary characteristic that even better takes the nature of overlapping tree canopies and remote-sensing data into account is the *spherical contact distribution function*, $H_S(r)$. As part of the estimation process, all parts of the observation window that are covered by tree crowns form one, united random set X (see the grey area in Figure 3(b)), whilst the gaps in between, where there is no tree biomass, is the complement of X (Pommerening and Grabarnik 2019, 103). The density variant of this function, $h_S(r)$, gives the density of the distances from arbitrary test locations ω outside X to the nearest points of X . As a result this function describes the size of gaps within the crown canopy patterns. $h_S(r)$ can be estimated in the same way as $d(r)$, i.e. using Equations (14) and (15), however, instead of considering distances between tree locations denoted as $\text{dist}(\xi)$, we

now analyse the aforementioned distances $\text{dist}_\omega(\xi)$ between test locations ω outside X and the nearest points of X (Chiu et al. 2013, 236). In addition, we also monitored the area fraction v of random set X , that is, the percentage of area covered by the union of tree crowns (see Figure 3(b)).

In addition to $d(r)$ and $h_5(r)$, we also used the aggregation index R' by Clark and Evans (1954) for monitoring the development of the spatial pattern of tree locations over time in the four simulation scenarios:

$$R' = \frac{\bar{r}}{\mathbf{E}r} \quad (16)$$

with $\mathbf{E}r = \frac{1}{2 \cdot \sqrt{\frac{N}{A}}}$ and $R' \in [0, 2.1491]$

This index compares the mean of simulated distances, \bar{r} , between any point of the pattern of tree locations and its first nearest neighbour with the corresponding expected value, that is, the mean distance in a corresponding Poisson point process, $\mathbf{E}r$. N and A are the number of points in the observation window and its area, respectively. $R' > 1$ indicates a tendency towards a regular (overdispersed) point pattern as caused by inhibition, whilst $R' < 1$ highlights a trend towards clustering (underdispersal) caused by mutual attraction. When mean simulated distance and mean Poisson distance are roughly the same, $R' \approx 1$. For calculating this index, we used the NN1 edge correction (Pommerening and Stoyan 2006).

Further we considered the *mark variogram* $\gamma_m(r)$, a characteristic derived from geostatistical variograms and designed for quantitative marks m such as plant size variables. Its test function $\frac{1}{2}(m(\xi_i) - m(\xi_j))^2$ quantifies the difference between two marks by subtracting them from one another and squaring the difference. The estimator of the mark variogram we used in this study is given in Equation (17).

$$\hat{\gamma}_m(r) = \frac{1}{\sigma_m^2} \sum_{\xi_i, \xi_j \in W}^{\#} \frac{\frac{1}{2}(m(\xi_i) - m(\xi_j))^2 k_h(\|\xi_i - \xi_j\| - r)}{2\pi r A(W_{\xi_i} \cap W_{\xi_j})} \quad (17)$$

The normalizing term before the sum is the reciprocal of the mark variance σ_m^2 and in our case crown diameters were the size marks m used. For homogeneous data, the non-normalized mark variogram converges towards σ_m^2 at larger distances. As this is also an important characteristic, we monitored σ_m^2 throughout the simulations. k_h is again the aforementioned Epanechnikov kernel. $A(W_{\xi_i} \cap W_{\xi_j})$ is the area of intersection of W_{ξ_i} and W_{ξ_j} , see Illian et al. (2008, 481 f. and p. 188), relating to the translational edge correction (Ohser and Stoyan 1981). Large differences between tree crowns are indicated by $\gamma_m(r) > 1$ (also referred to as negative association), whilst with $\gamma_m(r) < 1$ (also referred to as positive association) both crown radii are similar in size regardless whether the two radii in question are both large or both small. Spatially uncorrelated (= independent) crown radii are indicated by $\gamma_m(r) \approx 1$ (Suzuki, Kachi, and Suzuki 2008; Pommerening and Särkkä 2013).

Applying the GET package, we calculated the 50% central region around the mean of each of the aforementioned summary characteristics from the 500 simulations to illustrate the variability among the replications. This is common procedure in functional data analysis and in spatial statistics (Myllymäki and Mrkvička 2019). For all simulations and

calculations, we used our own R (version 3.5.1, R Development Core Team 2020) and C++ code and additionally applied the spatstat (Baddeley, Rubak, and Turner 2016) and GET packages (Myllymäki and Mrkvička 2019).

3. Results

3.1. Non-spatial measures

Canopy cover fraction v is a characteristic from random-set statistics and gives the proportion of forest stand area covered by tree crowns, see Section 2.1.2 and Figure 3 (b). As such v is a density measure based on tree crown biomass and can include no but also multiple crown overlaps. Comparing the canopy cover fraction graphs reveals in all scenarios an initially steep build-up of canopy cover up to 25 years reaching $v \approx 0.7$ (Figure 6). The same trend is also reflected by the sum of crown projection areas; however, the values here are usually much higher than v , as crown overlaps are not considered. Only in scenario C1S1, the initial maximum of v is markedly less than 0.7. The initial maximum is followed by one or a few severe disturbances reducing canopy cover fraction to a much lower level. These disturbances are caused by dramatic events of natural mortality. The new level is affected less severely by disturbances and differs between the four scenarios.

The S0 scenarios without superorganism formation (Figure 6(a) and 6(b)) and those including superorganism formation (Figure 6(c) and 6(d)) apparently form two groups with shared similarities within them. In scenario C0S0 (Figure 6(a)), the new level is situated at $v \approx 0.6$ and is fairly constant through time (when ignoring minor fluctuations). In scenario C1S0 (Figure 6(b)), the initial reduction goes down to almost $v \approx 0.4$, increases afterwards to remain at $v \approx 0.5$ from 60 years onwards. Interestingly, the level of the sum of crown projection areas after 25 years is a bit lower in scenario C1S0 than in C0S0. In scenario C0S1 (Figure 6(c)), the new level of canopy fraction after the initial disturbance keeps declining towards what possibly is a new level after 60 years of simulation at around $v \approx 0.4$. A particularly sharp drop after the initial canopy cover fraction maximum with hardly any fluctuations can be observed for scenario C1S1. After this the new level remains remarkably constant between 25 and 60 years at $v \approx 0.4$ to decrease further

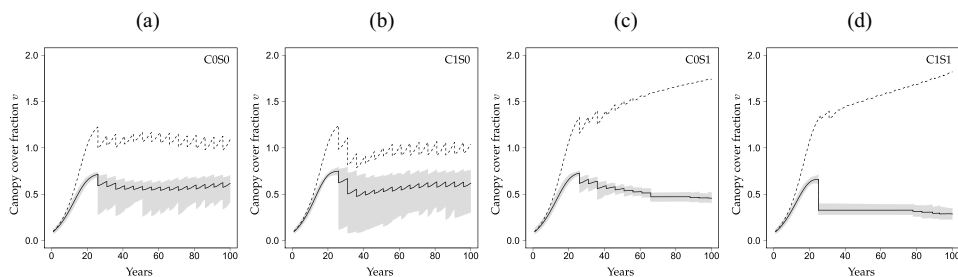


Figure 6. The development of crown canopy fraction v over time for the four simulation scenarios C0S0, C1S0, C0S1 and C1S1, see Section 2.5. The mean of 500 simulations is depicted as continuous line along with the shaded 50% central region of all 500 simulated v . The dashed line gives the total crown area, that is, the sum of all individual crown projection areas, divided by the area of the observation window for comparison.

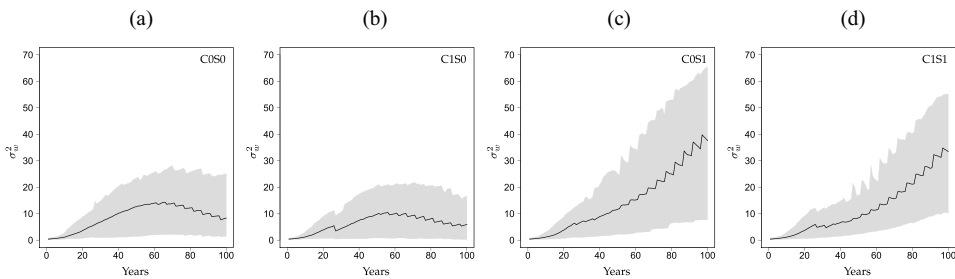


Figure 7. The development of crown-diameter variance σ_w^2 over time for the four simulation scenarios C0S0 (a), C1S0 (b), C0S1 (c) and C1S1 (d), see Section 2.5. The mean of 500 simulations is shown as continuous line along with the shaded 50% central region of all 500 simulated σ_w^2 .

afterwards towards $v \approx 0.3$ at 100 years of simulation. These results seem to suggest that both crown movement and superorganism formation reduce canopy cover fraction with the latter having a greater effect than the former. Both processes in combination (C1S1) cause a complementary effect leading to a markedly reduced canopy fraction. In scenarios with superorganism formation (Figure 6(c) and (d)), variation of simulations is markedly reduced compared to those where no superorganisms were allowed to form (Figure 6(a) and (b)). A comparison with the sum of crown projection areas of each individual tree relative to the area of the observation window shows that there is a long-term increase of crown area in both scenarios C0S1 and C1S1 while the canopy fraction keeps declining. Note that the long-term sum of crown projection areas is much lower in the two S0 than in the two S1 scenarios.

Another interesting characteristic is the crown radius variance σ_w^2 acting as an asymptote for the mark variogram at large distances r , see Section 2.6. Also here we can clearly see a divide between the scenarios with and without superorganism formation (Figure 7 (c) and (d) as opposed to Figure 7(a) and (b)). Whilst without superorganism formation σ_w^2 increases to reach a maximum of $\sigma_w^2 \approx 10 \text{ m}^2$ at around 60 years for scenarios C0S0 and C1S0 and then decreases again, there is a continued exponential increase of σ_w^2 throughout the simulation period in scenarios C0S1 and C1S1. The maximum of σ_w^2 at around 60 years is a bit lower in C1S0 compared to that in C0S0. In the latter scenarios, the variability in the simulation also increases exponentially with years.

Apparently the formation of superorganisms much increases the variability of the size of tree crowns, whilst with crown movements σ_w^2 remains comparatively low.

3.2. Spatially explicit characteristics

The nearest-neighbour distance distribution $d(r)$ provides spatial information on the distance patterns in the vicinity around each tree. Ten years after the beginning of the simulations, the estimated density distribution $\hat{d}(r)$ is still close to that of a Poisson point pattern (Figure 8), which in fact was used for initialization, see Section 2.4. Scenario C1S1 is an exception, since a bimodal distribution has formed already after 10 years of simulation. As expected, with increasing years, the differences between simulated and Poisson nearest-neighbour distance densities increase. These differences are particularly large

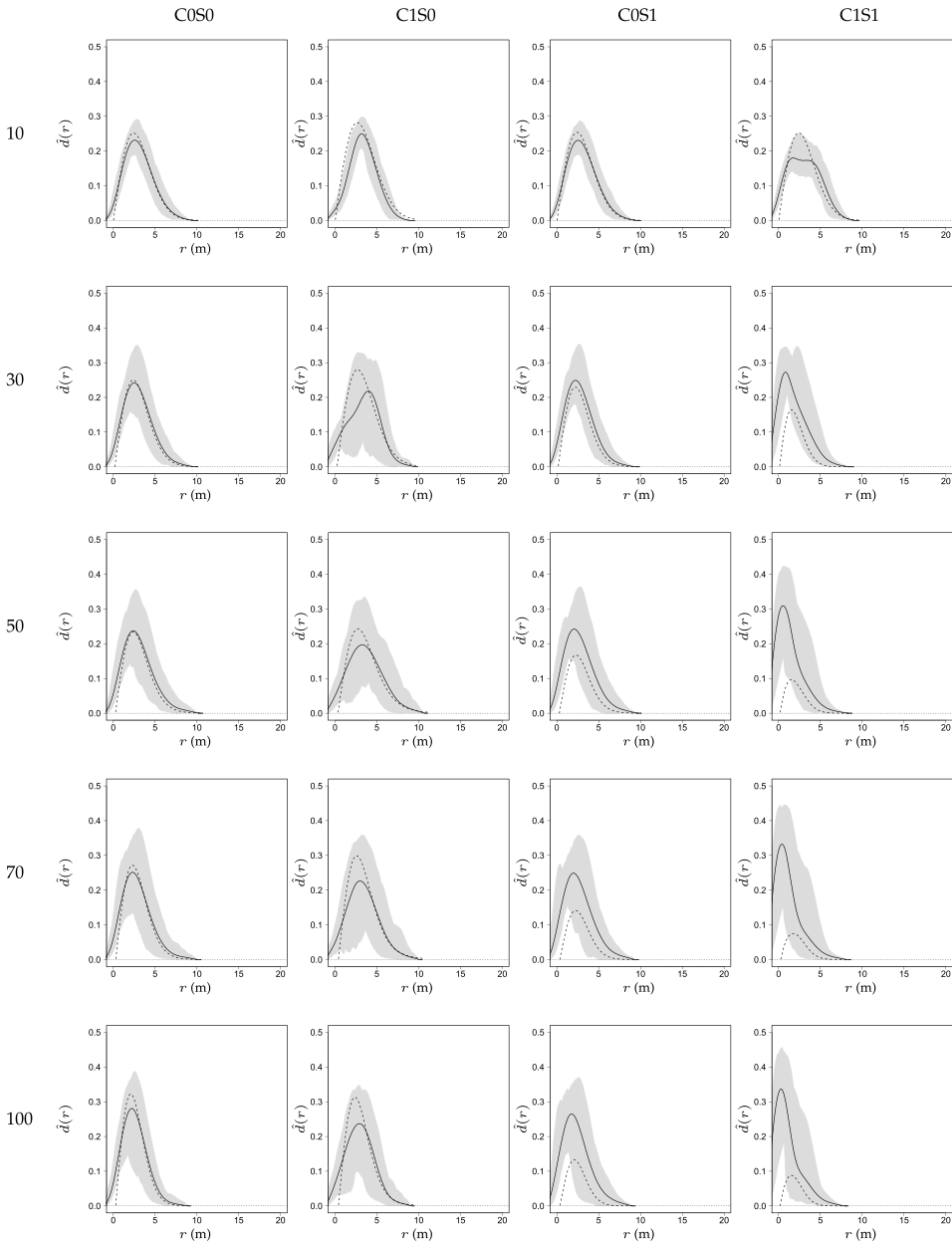


Figure 8. Estimations of the nearest-neighbour distance density function $\hat{d}(r)$ for the four simulation scenarios C0S0, C1S0, C0S1 and C1S1, see Section 2.5, and simulation years 10, 30, 50, 70, and 100 (continuous line). Corresponding $\hat{d}(r)$ for the case that all tree locations form a Poisson point process are shown as dotted lines. The lines are the means of 500 simulations and the shaded areas represent the 50% central region of all 500 simulated $\hat{d}(r)$.

for scenarios C0S1 and C1S1, that is, again for those scenarios where the formation of superorganisms was involved. However, the range of nearest-neighbour distances does not change much over the years.

It is striking that for scenarios C0S1 and C1S1, the $\hat{d}(r)$ distributions are shifted markedly further to the left than those related to scenarios C0S0 and C1S0. This trend is stronger for C1S1 than for C0S1. A small difference between scenarios C0S0 and C1S0 is the tendency that the distance density distributions related to C1S0 are slightly flatter and in year 30 a bimodal distribution can be observed. The nearest-neighbour distance distribution indicates that – as expected – the formation of superorganisms leads to spatial tree patterns with short nearest-neighbour distances and clustering (additionally confirmed in Figure 9), whilst crown shifts appear to increase nearest-neighbour distances. The effect of superorganism formation, was, however, much stronger than the effect of crown shifts and in scenario C1S1, contrary to our expectation, the superorganism effect was even enhanced by crown shifting.

The results of the analysis using the aggregation index by Clark and Evans (1954) confirmed that with crown plasticity (scenario C1S0) as expected there is a moderate tendency for $R' > 1$ which occasionally recovers from disturbances by birth and death events, whilst in the presence of superorganisms (scenarios C0S1 and C1S1), there is strong evidence of clustering $R' < 1$ of trees, particularly in scenario C1S1 (Figure 9(d)). Here, again crown plasticity and superorganism formation appear to complement their effects. As expected complete spatial randomness with $R' \approx 1$ occurs in the reference scenario C0S0 (see Figure 9(a)). Crown plasticity as implemented in our model leads to moderate regularity of tree locations whilst the formation of superorganisms results in strong clustering.

The spherical contact density function $h_S(r)$ sheds light on gap dynamics. The larger the range of the distribution the larger the associated gaps in the tree canopy pattern. Whilst the spherical contact density functions of the four scenarios are all quite similar in year 10, there are again marked differences between C0S0 and C1S0 on one hand and C0S1 and C1S1 on the other in years 50–100 (Figure 10).

In scenarios C0S1 and C1S1, beginning in year 50 the $\hat{h}_S(r)$ curves gradually flatten out until they stretch towards a gap diameter of more than 15 m in year 100. Again, crown plasticity in scenario C1S1 had a complementary effect on gap formation, as the range of $\hat{h}_S(r)$ is larger and the curve flatter in scenario C1S1 than in scenario C0S1. There was not much difference between scenarios C0S0 and C1S0. Crown plasticity is expected to decrease gap size, as this process leads to greater regularity of tree locations, but we

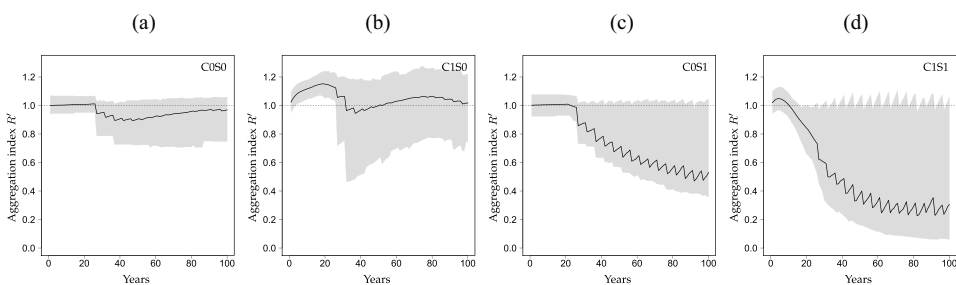


Figure 9. The development of the aggregation index R' (Clark and Evans 1954) over time for the four simulation scenarios C0S0 (a), C1S0 (b), C0S1 (c) and C1S1 (d), see Section 2.5. The mean of 500 simulations is depicted as continuous line along with the shaded 50% central region of all 500 simulated R' .

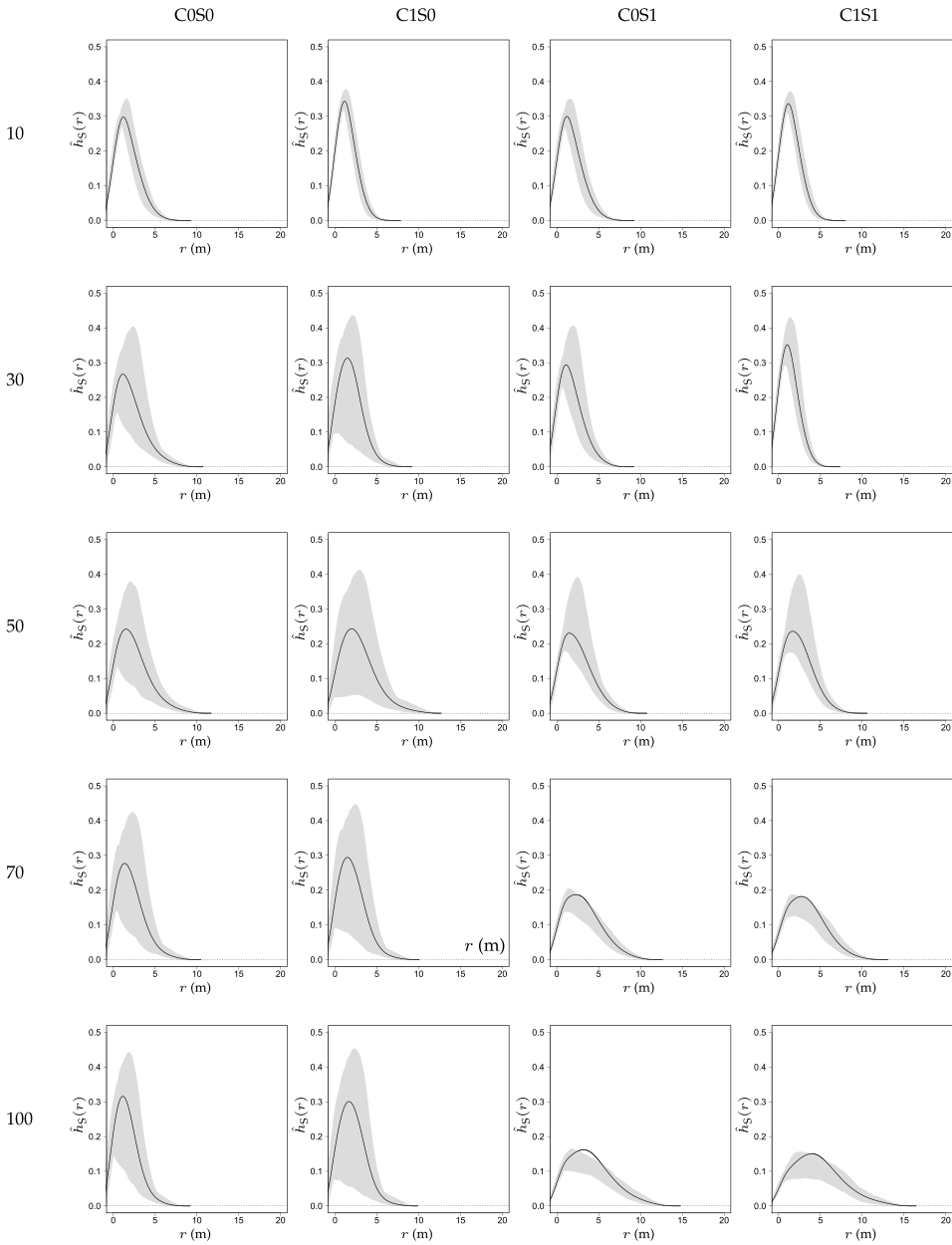


Figure 10. Estimations of the spherical contact density function $\hat{h}_S(r)$ for the four simulation scenarios C0S0, C1S0, C0S1 and C1S1, see Section 2.5, and simulation years 10, 30, 50, 70 and 100 (continuous line). The lines are the means of 500 simulations and the shaded areas represent the 50% central region of all 500 simulated $\hat{h}_S(r)$.

did not find much difference compared to scenario C0S0. Overall, we found that super-organism formation increases gap size whilst crown shift had hardly any effect on the gaps in the tree canopy.

In our study, the mark variogram considers tree crown diameters in addition to crown locations (Figure 11). In scenario C0S0, the mark variogram indicates positive association of crown diameters throughout the 100 years of simulation, that is, crown diameters are similar, particularly at shorter distances between $r = 0 - 20\text{m}$. This usually reflects patterns of small trees with comparatively small crown diameters.

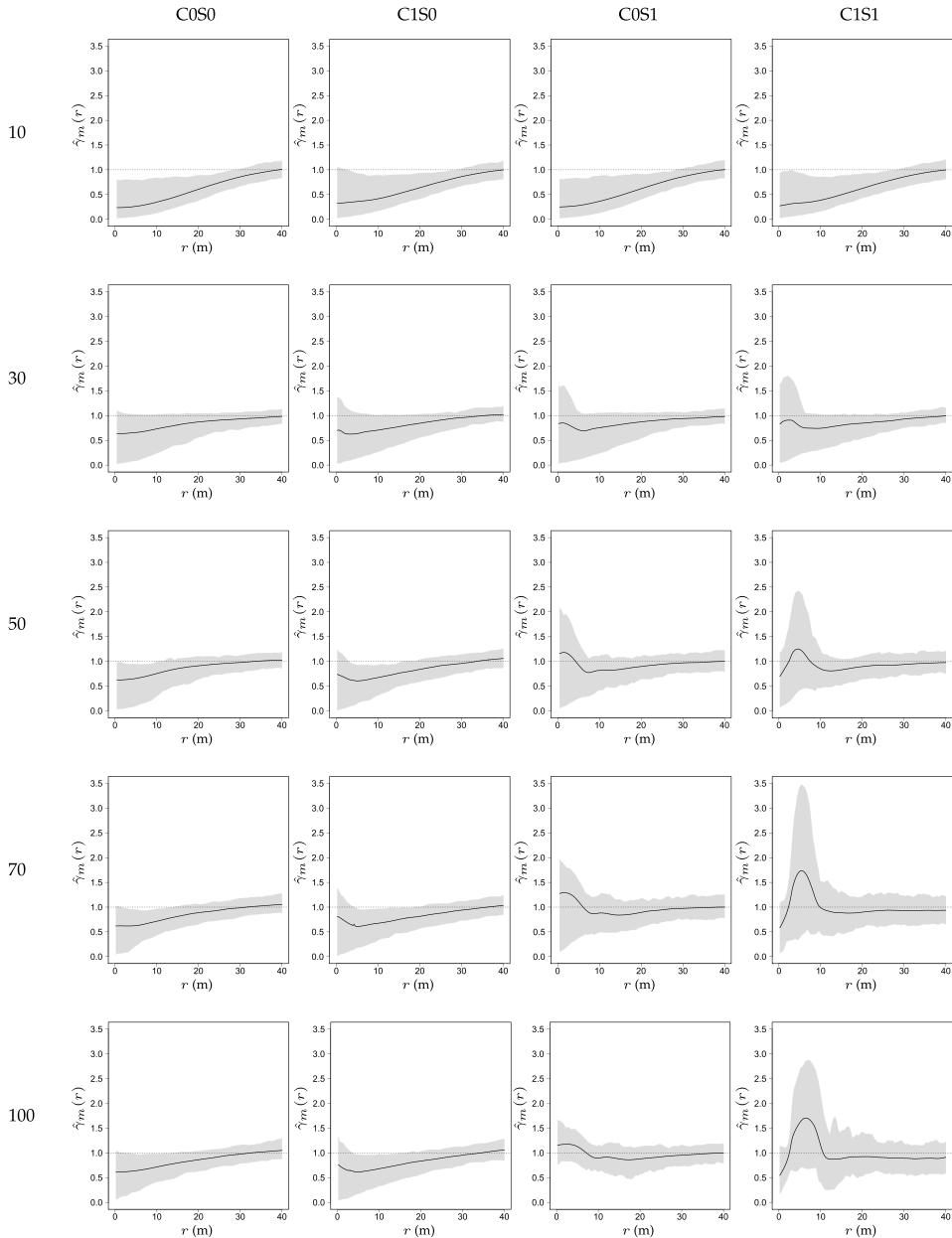


Figure 11. Estimations of the mark variogram $\hat{\gamma}_m(r)$ for the four simulation scenarios C0S0, C1S0, C0S1 and C1S1, see Section 2.5, and simulation years 10, 30, 50, 70 and 100 (continuous line). The lines are the means of 500 simulations and the shaded areas represent the 50% central region of all 500 simulated $\hat{\gamma}_m(r)$.

The effect of positive mark association is particularly strong at the beginning in simulation year 10 and then weakens by approaching the horizontal line through 1 with a similar trend in all subsequent years. Scenario C150 reveals much the same general tendency as C050, however, beginning with year 50, there is a small rise of the $\hat{\gamma}_m(r)$ curve towards 1 between $r = 0 - 5$ m. In this range, there is a slight tendency of neighbouring crown diameters to be closer to a situation where there is no correlation between crown diameters. This trend is even more developed in scenario C051 starting in year 30 to eventually take values of $\hat{\gamma}_m(r) > 1$ qualifying for negative association of crown diameters. This range of negative mark association stretches as far as $r \approx 10$ m implying that trees in this distance range have very different crown diameters. The effect of negative association of crown diameter is, however, strongest in scenario C151. Initially, there is positive mark association up to $r = 3$ m followed by a maximum of negative association around $r = 6$ m. Naturally, the variability of the mark variogram is greatest for short distances, as a gradual convergence towards 1 is expected for large r . Particularly large variability can be observed for scenario C151 around the maximum of negative mark association. Apparently, the formation of superorganisms plays a dividing role also in terms of the mark variogram: At distances $r < 12$ m positive mark association (with similar crown diameters) dominates in the scenarios without superorganism formation whilst negative association (with dissimilar crown diameters) prevails in this range when superorganisms are allowed to form in the simulations.

4. Discussion

CanopyShotNoise is the prototype of a dynamic forest model designed to be used with data directly derived from remote sensing. In this study, we presented *CanopyShotNoise* as a first step towards bridging the gap between individual-based forest modelling and remote sensing (see [Figures 1 and 3\(b\)](#)). Therefore, the model focus is on tree canopies and the model relies on modern concepts from point process and random set statistics. *CanopyShotNoise* can not only be used to project future forest development but also, and perhaps more importantly, for experimentation to answer urgent ecological questions. ALS remote sensing has become one of the most important remote-sensing data source in forest monitoring and it can be assumed that more multi-temporal ALS datasets will become available. Furthermore, the development in LiDAR sensor technologies with increasing repetition rates and multiple wavelengths as well as the integration of LiDAR sensors into unmanned aerial systems (UAS) will improve the availability and quality of high-resolution point clouds even more and thus the opportunity to produce single tree locations and tree crown shapes for large areas in an efficient manner.

The *CanopyShotNoise* model requires tree coordinates; however, the detection probability of single trees is dependent on their size and vertical position. Smaller understorey trees usually have a considerably lower chance to be detected (Heurich et al. 2004; Korpela, Hovi, and Morsdorf 2012; Persson, Holmgren, and Söderman 2002). The expected increase in point densities together with new approaches that perform individual tree detection directly on the unstructured point cloud (e.g. Yao, Krzystek, and Heurich 2013) might reduce the problem of undetected understorey trees (Hamraz, Contreras, and Zhang 2017).

In this study, we explored the phenomena of crown plasticity (C) and superorganisms (S) through model simulations based on *CanopyShotNoise*. These two phenomena have only recently gained research attention in forest ecology (Gavrikov, Grabarnik, and Stoyan 1993; García 2014; Gorzelak et al. 2015; Pommerening and Uria-Diez 2017; Till-Bottraud, Fajardo, and Rioux 2012; Schröter, Härdtle, and von Oheimb 2012; Vovides et al. 2018). We compared combinations of crown plasticity and superorganisms in four scenarios, that is, C0S0, C1S0, C0S1 and C1S1, and hypothesized that crown plasticity would lead to greater regularity of tree locations whilst antagonistically the formation of superorganisms would encourage clustering.

Our simulation results indeed suggested that distances between trees in the long run tend to decrease (Figure 8) and gap size to increase (Figure 10) when superorganisms are encouraged to form. As a consequence tree canopy cover fraction decreases (Figure 6). On first glance, this could be interpreted as a decreasing carrying capacity but in fact carrying capacity did not decrease in our simulations and in the two S1 scenarios the total canopy area even increased with time. The formation of superorganisms typically leads to a situation where tree crowns are more densely packed, thus making space for larger gaps. This is also reflected by the low numbers of the aggregation index (Clark and Evans 1954; Figure 9(c) and (d)). The increased packing of tree crowns can, therefore, be seen as an extreme form of facilitation in an attempt to adapt to environmental challenges particularly in forest ecosystems with shade-tolerant species such as *F. sylvatica*. This can be explained by the fact that smaller trees have a better chance of survival under the protection of larger individuals whilst being dominated by them at the same time. The formation of superorganisms also dramatically increases the variability of crown size (Figure 7). It is interesting to note that crown biomass production is much larger and increasing in the S1 scenarios compared to the S0 scenarios where crown biomass production is low and remains roughly constant.

Crown plasticity was hypothesized to lead to regular patterns of tree dispersal, since regularity is an efficient way to grant space to each individual. Therefore, we monitored the aggregation index by Clark and Evans (1954, see Figure 9). Here, we found that there is indeed a clear trend toward more regularity in scenario C1S0 (Figure 9(b)) compared to reference scenario C0S0 (Figure 9(a)). However, this trend was weaker than we expected. In Figure 9(b), the sudden drop in the aggregation index around 25 years of simulation coincides with the sudden drop in canopy cover fraction (Figure 6(b)). Apparently, the large mortality disturbance after 25 years of simulation contributed to a dramatic reduction in the aggregation index and the former values only slowly and not completely recovered thereafter. In scenario C0S1, there is a dramatic and continued decline in the aggregation index after the initial 25 years of simulation illustrating the strength of the superorganism effect whilst in C1S1, this trend is even more dramatic and starts already in year 10. It is also interesting to note the considerable variation in both the aggregation index and the canopy cover fraction after simulation year 25. The reasons for the moderate regularity of tree dispersal in scenario C1S0 can be explained by the fact that the trees attempt to evade competition pressure that is passed on to them by the shot-noise field and not so much evaded other trees directly. In the shot-noise field, neighbouring trees with larger size carry a higher weight than smaller trees. This is also likely to contribute to deviations from regularity. At the same time, repeated birth events reduce the aggregation index, since they introduce clusters.

We also hypothesized that crown plasticity – as a consequence of imposing more regular tree locations – would decrease gap size, but there was no evidence supporting this hypothesis (Figure 9, C1S0). Surprisingly despite the extreme setting for $R = 0.4$ m (see Section 2.5), shifting tree crowns had hardly any influence on gap dynamics, as measured by $\hat{h}_S(r)$.

The complementarity or interaction effect between crown plasticity and superorganism formation in scenario C1S1 is noteworthy. The effect causes smaller mean nearest-neighbour distances (Figure 8) and larger mean gap diameters (Figure 9), particularly in simulation years 70 and 100, than in scenario C0S1. The interaction effect is also evident in the patterns of the aggregation index (Figure 9(c) and (d)). It is possible that the stronger effect of superorganism formation decreases the majority of nearest-neighbour distances whilst the few remaining independent individuals attempt to keep their distance to the superorganisms but available space for evasion is in short supply at this stage. It is also plausible that the competition pressure is too high for individuals to move into gaps between two or three superorganisms and therefore remain at their current location. This phenomenon definitely requires further analysis in future studies.

The mark variogram highlighted that the formation of superorganisms strongly supports negative association or negative autocorrelation of tree crowns implying that the size of crowns differ a lot around a distance of 5 m starting with simulation year 50 (Figure 11). Negative association of quantitative tree variables in spatial patterns is comparatively rare (Pommerening and Särkkä 2013). This likely results from the fact that small trees are in this scenario encouraged to persist and can survive in greater numbers in the vicinity of large trees. Interestingly, also crown movements lead to more diversity in crown sizes at close proximity, see scenario C1S0 compared to C0S0 in Figure 11. However, this effect is much weaker than the effect caused by the formation of superorganisms in scenarios C0S1 and C1S1. The differences in the mark variograms between the S1 and the S0 scenarios can also partly be explained by the fact that with the S1 scenarios the variance of crown diameters increased exponentially by year, that is the chances of pairings with differing crown diameters at close proximity were much higher in the S1 scenarios (Figure 7).

5. Conclusions

With the *CanopyShotNoise* IBM, we present a dynamic forest model that can be directly interfaced with information derived from ALS remote-sensing data. Using this model, our simulations revealed that the formation of superorganisms has a stronger effect on spatial tree and canopy patterns than crown plasticity. The former process leads to clusters with denser, more compact packing of tree canopies and opens larger gaps between the clusters. Crown plasticity on the other hand introduced a greater regularity between tree locations; however, this process apparently has little effect on gap dynamics. There was a curious interaction between the formation of superorganisms and crown plasticity leading to even greater gaps than in a scenario where superorganisms acted alone. The formation of superorganisms also substantially increased crown-size diversity and strong negative spatial association between crown diameters, a rare phenomenon was indicated by the mark variogram as a consequence of this process. With ongoing climate change, it is likely that facilitation between trees will increase and as a consequence we are likely to

observe spatial patterns in our monitoring that resemble the patterns found in our superorganism model simulations. Our and similar studies can then aid correct interpretation of monitoring results.

Acknowledgements

The authors thank Pavel Grabarnik (Russian Academy of Sciences, Russia) for helpful and much appreciated comments on our description of the nearest-neighbour distance and the spherical contact density functions whilst Mikko Kuronen (Natural Resources Institute Finland, LUKE) kindly provided efficient R implementations for these functions. Christoph Kleinn granted the first author office space and access to printers at his Chair of Forest Inventory and Remote Sensing (Göttingen University, Germany) during the challenging COVID-19 crisis and Hendrik Heydecke from the same institution supported us by kindly printing drafts of the manuscript and engaging the first author in pleasant discussions. *Fagus sylvatica* time-series data were gratefully received from Andreas Zingg (Swiss Federal Institute for Forest, Snow and Landscape Research WSL, Birmensdorf, Switzerland).

Disclosure statement

The authors declare that they have no known financial interests or personal relationships that could have influenced the work reported in this paper.

Data accessibility

The *CanopyShotNoise* model source code used in this study is available at <https://zenodo.org/record/5035424> or using DOI 10.5281/zenodo.5035424.

Authors' contributions

All authors analysed the data, carried out the modelling/analyses and substantially contributed to the text. All persons entitled to co-authorships have been included in this paper. All authors have seen and approved the submitted version of the manuscript.

Funding

MM was financially supported by the Academy of Finland (project numbers 295100 and 327211) under the UNITE flagship ecosystem.

ORCID

Arne Pommerening  <http://orcid.org/0000-0002-3441-2391>

References

Adams, T., G. Ackland, G. Marion, and C. Edwards. 2011. "Understanding Plantation Transformation Using a Size-structured Spatial Population Model." *Forest Ecology and Management* 261 (3): 799–809. doi:10.1016/j.foreco.2010.10.036.

- Bacelli, F., and B. Blaszczyzyn. 2001. "On a Coverage Process Ranging from the Boolean Model to the Poisson-Voronoi Tessellation." *Advances in Applied Probability* 33 (2): 293–323. doi:10.1017/S0001867800010806.
- Baddeley, A., E. Rubak, and R. Turner. 2016. "Spatial Point Patterns." *Methodology and Applications with R*. Boca Raton: CRC Press.
- Berger, U., and H. Hildenbrandt. 2000. "A New Approach to Spatially Explicit Modelling of Forest Dynamics: Spacing, Ageing and Neighbourhood Competition of Mangrove Trees." *Ecological Modelling* 132 (3): 287–302. doi:10.1016/S0304-3800(00)00298-2.
- Bertness, M. D., and R. Callaway. 1994. "Positive Interactions in Communities." *Trends in Ecology and Evolution* 9 (5): 191–193. doi:10.1016/0169-5347(94)90088-4.
- Bolker, B. M. 2008. *Ecological Models and Data in R*. Princeton: Princeton University Press.
- Bolton, D. K., J. C. White, M. A. Wulder, N. C. Coops, T. Hermosilla, and X. Yuan. 2018. "Updating Stand-level Forest Inventories Using Airborne Laser Scanning and Landsat Time Series Data." *International Journal of Applied Earth Observation and Geoinformation* 66: 174–183. doi:10.1016/j.jag.2017.11.016.
- Cade, B. S., and B. R. Noon. 2003. "A Gentle Introduction to Quantile Regression for Ecologists." *Frontiers in Ecology and the Environment* 1 (8): 412–420. doi:10.1890/1540-9295(2003)001[0412:AGITQR]2.0.CO;2.
- Chiu, S. N., D. Stoyan, W. S. Kendall, and J. Mecke. 2013. *Stochastic Geometry and Its Applications*. 3rd ed. Chichester: John Wiley & Sons.
- Clark, P. J., and F. C. Evans. 1954. "Distance to Nearest Neighbour as a Measure of Spatial Relationships in Populations." *Ecology* 35 (4): 445–453. doi:10.2307/1931034.
- Cronie, O., K. Nyström, and J. Yu. 2013. "Spatiotemporal Modeling of Swedish Scots Pine Stands." *Forest Science* 9 (5): 505–516. doi:10.5849/forsci.12-007.
- Falkowski, M. J., A. T. Hudak, N. L. Crookston, P. E. Gessler, E. H. Uebler, and A. M. S. Smith. 2010. "Landscape-scale Parameterization of a Tree-level Forest Growth Model: A K-nearest Neighbor Imputation Approach Incorporating LiDAR Data." *Canadian Journal of Forest Research* 40 (2): 184–199. doi:10.1139/X09-183.
- Falster, D. S., and M. Westoby. 2003. "Plant Height and Evolutionary Games." *Trends in Ecology and Evolution* 18 (7): 337–343. doi:10.1016/S0169-5347(03)00061-2.
- García, O. 2014. "Can Plasticity Make Spatial Structure Irrelevant in Individual-tree Models?" *Forest Ecosystems* 1 (1): 16. doi:10.1186/s40663-014-0016-1.
- Gavrikov, V., P. Grabarnik, and D. Stoyan. 1993. "Trunk-top Relations in a Siberian Pine Forest." *Biometrical Journal* 35 (4): 487–498. doi:10.1002/bimj.4710350412.
- Gorzalak, M. A., A. K. Asay, B. J. Pickles, and S. W. Simard. 2015. "Inter-plant Communication through Mycorrhizal Networks Mediates Complex Adaptive Behaviour in Plant Communities." *AoB Plants* 7: plv050. doi:10.1093/aobpla/plv050.
- Gregoire, T. G., and H. T. Valentine. 2008. *Sampling Strategies for Natural Resources and the Environment*. *Applied Environmental Statistics*. Boca Raton: Chapman & Hall/CRC.
- Häbel, H., M. Myllymäki, and A. Pommerening. 2019. "New Insights on the Behaviour of Alternative Types of Individual-based Tree Models for Natural Forests." *Ecological Modelling* 406: 23–32. doi:10.1016/j.ecolmodel.2019.02.013.
- Hamraz, H., M. A. Contreras, and J. Zhang. 2017. "Forest Understorey Trees Can Be Segmented Accurately within Sufficiently Dense Airborne Laser Scanning Point Clouds." *Scientific Reports* 7 (1): 1–9. doi:10.1038/s41598-017-07200-0.
- Hanisch, K.-H. 1984. "Some Remarks on Estimators of the Distribution Function of Nearest Neighbour Distance in Stationary Spatial Point Processes." *Mathematische Operationsforschung und Statistik – Statistics* 15: 409–412.
- Heidrich, L., S. Bae, S. Levick, S. Seibold, W. Weisser, P. Krzystek, P. Magdon, et al.. 2020. "Heterogeneity–diversity Relationships Differ between and within Trophic Levels in Temperate Forests." *Nature Ecology and Evolution* 4 (9): 1204–1212. DOI:10.1038/s41559-020-1245-z.
- Heurich, M., Å. Persson, J. Holmgren, and E. Kennel. 2004. "Detecting and Measuring Individual Trees with Laser Scanning in Mixed Mountain Forest of Central Europe Using an Algorithm." *The*

- International Archives of the Photogrammetry*, 307–312. Remote Sensing and Spatial Information Sciences XXXVI.
- Ho, L. P., and D. Stoyan. 2008. "Modelling Marked Point Patterns by Intensity-marked Cox Processes." *Statistics & Probability Letters* 78 (10): 1194–1199. doi:10.1016/j.spl.2007.11.013.
- Iglhaut, J., C. Cabo, S. Puliti, L. Piermattei, J. O'Connor, and J. Rosette. 2019. "Structure from Motion Photogrammetry in Forestry: A Review." *Current Forestry Reports* 5 (3): 155–168. doi:10.1007/s40725-019-00094-3.
- Illian, J., A. Penttinen, H. Stoyan, and D. Stoyan. 2008. *Statistical Analysis and Modelling of Spatial Point Patterns*. Chichester: John Wiley & Sons.
- Jung, K., S. Kaiser, S. Böhm, J. Nieschulze, and E. K. V. Kalko. 2012. "Moving in Three Dimensions: Effects of Structural Complexity on Occurrence and Activity of Insectivorous Bats in Managed Forest Stands." *Journal of Applied Ecology* 49 (2): 523–531. doi:10.1111/j.1365-2664.2012.02116.x.
- Koenker, R., and B. J. Park. 1994. "An Interior Point Algorithm for Nonlinear Quantile Regression." *Journal of Econometrics* 71 (1–2): 265–283. doi:10.1016/0304-4076(96)84507-6.
- Korpela, I., A. Hovi, and F. Morsdorf. 2012. "Understorey Trees in Airborne LiDAR Data - Selective Mapping Due to Transmission Losses and Echo-triggering Mechanisms." *Remote Sensing of Environment* 119: 92–104. doi:10.1016/j.rse.2011.12.011.
- LeMay, V., A. Pommerening, and P. Marshall. 2009. "Spatio-temporal Structure of Multi-storied, Multi-aged Interior Douglas Fir (*Pseudotsuga Menziesii* Var. *Glauca*) Stands." *Journal of Ecology* 97 (5): 1062–1074. doi:10.1111/j.1365-2745.2009.01542.x.
- Li, W., Q. Guo, M. K. Jakubowski, and M. Kelly. 2012. "A New Method for Segmenting Individual Trees from the Lidar Point Cloud." *Photogrammetric Engineering and Remote Sensing* 78 (1): 75–84. doi:10.14358/PERS.78.1.75.
- Ma, Q., Y. Su, S. Tao, and Q. Guo. 2018. "Quantifying Individual Tree Growth and Tree Competition Using Bi-temporal Airborne Laser Scanning Data: A Case Study in the Sierra Nevada Mountains, California." *International Journal of Digital Earth* 11 (5): 485–503. doi:10.1080/17538947.2017.1336578.
- Magnussen, S., T. Nord-Larsen, and T. Riis-Nielsen. 2018. "Lidar Supported Estimators of Wood Volume and Aboveground Biomass from the Danish National Forest Inventory (2012–2016)." *Remote Sensing of Environment* 211: 146–153. doi:10.1016/j.rse.2018.04.015.
- Marczak, P. T., K. Y. van Ewijk, P. M. Treitz, N. A. Scott, and D. C. E. Robinson. 2020. "Predicting Carbon Accumulation in Temperate Forests of Ontario, Canada Using a LiDAR-initialized Growth-and-yield Model." *Remote Sensing* 12 (1): 201. doi:10.3390/rs12010201.
- Michaelis, M., and M. L. Menten. 1913. "Die Kinetik Der Invertinwirkung." ["the Kinetics of Invertase Action."]. *Biochemische Zeitschrift* 49: 333–369.
- Miina, J., and T. Pukkala. 2002. "Application of Ecological Field Theory in Distance-dependent Growth Modelling." *Forest Ecology and Management* 161 (1–3): 101–107. doi:10.1016/S0378-1127(01)00489-3.
- Müller, J., C. Moning, C. Bässler, M. Heurich, and R. Brandl. 2009. "Using Airborne Laser Scanning to Model Potential Abundance and Assemblages of Forest Passerines." *Basic and Applied Ecology* 10 (7): 671–681. doi:10.1016/j.baae.2009.03.004.
- Myllymäki, M., and A. Penttinen. 2009. "Conditionally Heteroscedastic Intensity-dependent Marking of Log Gaussian Cox Processes." *Statistica Neerlandica* 63 (4): 450–473. doi:10.1111/j.1467-9574.2009.00433.x.
- Myllymäki, M., and T. Mrkvička. 2019. "GET: "Global Envelopes in R." arXiv:1911.06583 [Stat.me]."
- Næsset, E. 2014. "Area-based Inventory in Norway – From Innovation to an Operational Reality." In *Forestry Applications of Airborne Laser Scanning*, M. Maltamo, E. Næsset, and J. Vauhkonen edited by, Vol. 27, 215–240. Managing Forest Ecosystems. Dordrecht: Springer.
- Nakamura, A., R. L. Kitching, M. Cao, T. J. Creedy, T. M. Fayle, M. Freiberg, C. N. Hewitt, et al.. 2017. "Forests and Their Canopies: Achievements and Horizons in Canopy Science." *Trends in Ecology and Evolution* 32 (6): 439–451. DOI:10.1016/j.tree.2017.02.020.
- Nanos, N., K. Larson, M. Millerón, and S. Sjöstedt-de Luna. 2010. "Inverse Modelling for Effective Dispersal: Do We Need Tree Size to Estimate Fecundity?" *Ecological Modelling* 221 (20): 2415–2424. doi:10.1016/j.ecolmodel.2010.07.004.

- Nilsson, M., K. Nordkvist, J. Jonzén, N. Lindgren, P. Axensten, J. Wallerman, M. Egberth, et al.. 2017. "A Nationwide Forest Attribute Map of Sweden Predicted Using Airborne Laser Scanning Data and Field Data from the National Forest Inventory". *Remote Sensing of Environment* 194: 447–454. doi:10.1016/j.rse.2016.10.022.
- Ohser, J., and D. Stoyan. 1981. "On the Second-order and Orientation Analysis of Planar Stationary Point Processes." *Biometrical Journal* 23 (6): 523–533. doi:10.1002/bimj.4710230602.
- Packalen, P., T. Pukkala, and A. Pascual. 2020. "Combining Spatial and Economic Criteria in Tree-level Harvest Planning." *Forest Ecosystems* 7: 18.
- Pascual, A. 2021. "Multi-objective Forest Planning at Tree-level Combining Mixed Integer Programming and Airborne Laser Scanning." *Forest Ecology and Management* 483: 118714. doi:10.1016/j.foreco.2020.118714.
- Perry, D. A., R. Oren, and S. C. Hart. 2008. *Forest Ecosystems*. 2nd ed. Baltimore: Johns Hopkins University Press.
- Persson, Å., J. Holmgren, and U. Söderman. 2002. "Detecting and Measuring Individual Trees Using an Airborne Laser Scanner." *Photogrammetric Engineering and Remote Sensing* 68: 925–932.
- Pommerening, A., J. Uria-Diez, 2017. "Do Large Forest Trees Tend towards High Species Mingling?" *Ecological Informatics* 42, 139–147
- Pommerening, A., and A. Muszta. 2016. "Relative Plant Growth Revisited: Towards a Mathematical Standardisation of Separate Approaches." *Ecological Modelling* 320: 383–392. doi:10.1016/j.ecolmodel.2015.10.015.
- Pommerening, A., and A. Särkkä. 2013. "What Mark Variograms Tell about Spatial Plant Interactions." *Ecological Modelling* 251: 64–72. doi:10.1016/j.ecolmodel.2012.12.009.
- Pommerening, A., and A. J. Sánchez Meador. 2018. "Tamm Review: "Tree Interactions between Myth and Reality"." *Forest Ecology and Management* 428: 164–176. doi:10.1016/j.foreco.2018.04.051.
- Pommerening, A., and D. Stoyan. 2006. "Edge-correction Needs in Estimating Indices of Spatial Forest Structure." *Canadian Journal of Forest Research* 36 (7): 1723–1739. doi:10.1139/x06-060.
- Pommerening, A., and P. Grabarnik. 2019. *Individual-based Methods of Forest Ecology and Management*. Cham: Springer.
- Pommerening, A., V. LeMay, and D. Stoyan. 2011. "Model-based Analysis of the Influence of Ecological Processes on Forest Point Pattern Formation – A Case Study." *Ecological Modelling* 222 (3): 666–678. doi:10.1016/j.ecolmodel.2010.10.019.
- Pont, D., H. S. Dungey, M. Suontama, and G. T. Stovold. 2021. "Spatial Models with Inter-Tree Competition from Airborne Laser Scanning Improve Estimates of Genetic Variance." *Frontiers in Plant Science* 11: 1–9. doi:10.3389/fpls.2020.596315.
- Pretzsch, H. 2009. *Forest Dynamics, Growth and Yield. From Measurement to Model*. Heidelberg: Springer.
- Purves, D. W., J. W. Lichstein, and S. W. Pacala. 2007. "Crown Plasticity and Competition for Canopy Space: A New Spatially Implicit Model Parameterized for 250 North American Species." *PloS One* 2 (9): e870. doi:10.1371/journal.pone.0000870.
- R Development Core Team. 2020. *R: A Language and Environment for Statistical Computing*. Vienna, Austria: R Foundation for Statistical Computing. <http://www.r-project.org> .
- Reitberger, J., M. Heurich, P. Krzystek, and U. Stilla. 2014. "Single Tree Detection in Forest Areas with High-density Lidar Data." *The International Archives of the Photogrammetry, Remote Sensing and Spatial Information Sciences* 36: 139–144.
- Renshaw, E., and A. Särkkä. 2001. "Gibbs Point Processes for Studying the Development of Spatial-temporal Stochastic Processes." *Computational Statistics & Data* 36 (1): 85–105. doi:10.1016/S0167-9473(00)00028-1.
- Särkkä, A., and E. Renshaw. 2006. "The Analysis of Marked Point Patterns Evolving through Space and Time." *Computational Statistics & Data* 51 (3): 1698–1718. doi:10.1016/j.csda.2006.07.008.
- Schröter, M., W. Härdtle, and G. von Oheimb. 2012. "Crown Plasticity and neighborhood Interactions of European Beech (*Fagus Sylvatica* L.) In an Old-growth Forest." *European Journal of Forest Research* 131 (3): 787–798. doi:10.1007/s10342-011-0552-y.

- Senf, C., D. Pflugmacher, Y. Zhiqiang, J. Sebal, J. Knorn, M. Neumann, P. Hostert, and R. Seidl. 2018. "Canopy Mortality Has Doubled in Europe's Temperate Forests over the Last Three Decades." *Nature Communications* 9 (1): 4978. doi:10.1038/s41467-018-07539-6.
- Shang, C., P. Treitz, J. Caspersen, and T. Jones. 2017. "Estimating Stem Diameter Distributions in a Management Context for a Tolerant Hardwood Forest Using ALS Height and Intensity Data." *Canadian Journal of Remote Sensing* 43 (1): 79–94. doi:10.1080/07038992.2017.1263152.
- Snyder, R. E., and P. Chesson. 2004. "How the Spatial Scales of Dispersal, Competition and Environmental Heterogeneity Interact to Affect Coexistence." *American Naturalist* 164 (5): 633–650. doi:10.1086/424969.
- Suzuki, S. N., N. Kachi, and J.-I. Suzuki. 2008. "Development of a Local Size Hierarchy Causes Regular Spacing of Trees in an Even-aged *Abies* Forest: Analyses Using Spatial Autocorrelation and the Mark Correlation Function." *Annals of Botany* 102 (3): 435–441. doi:10.1093/aob/mcn113.
- Till-Bottraud, I., A. Fajardo, and D. Rioux. 2012. "Multi-stemmed Trees of *Nothofagus Pumilio* Second-growth Forest in Patagonia are Formed by Highly Related Individuals." *Annals of Botany* 110 (4): 905–913. doi:10.1093/aob/mcs146.
- Tompalski, P., N. C. Coops, P. L. Marshall, J. C. White, M. A. Wulder, and T. Bailey. 2018. "Combining Multi-date Airborne Laser Scanning and Digital Aerial Photogrammetric Data for Forest Growth and Yield Modelling." *Remote Sensing* 10 (3): 347. doi:10.3390/rs10020347.
- Uria-Diez, J., and A. Pommerening. 2017. "Crown Plasticity in Scots Pine (*Pinus Sylvestris* L.) As a Strategy of Adaptation to Competition and Environmental Factors." *Ecological Modelling* 356: 117–126. doi:10.1016/j.ecolmodel.2017.03.018.
- Versace, S., D. Gianelle, L. Frizzera, R. Tognetti, V. Garfi, and M. Dalponte. 2019. "Prediction of Competition Indices in a Norway Spruce and Silver Fir-dominated Forest Using Lidar Data." *Remote Sensing* 11 (23): 2734. doi:10.3390/rs11232734.
- Vogt, D. R., D. J. Murrell, and P. Stoll. 2010. "Testing Spatial Theories of Plant Coexistence: No Consistent Differences in Intra- and Interspecific Interaction Distances." *The American Naturalist* 175 (1): 73–84. doi:10.1086/648556.
- Vovides, A., U. Berger, U. Grueters, R. Guevara, A. Pommerening, A. L. Lara-Domínguez, and J. López-Portillo. 2018. "Change in Drivers of Mangrove Crown Displacement along a Salinity Stress Gradient." *Functional Ecology* 32 (12): 2753–2765. doi:10.1111/1365-2435.13218.
- Wenk, G. 1972. "Zuwachsprögnosen, Vorratsfortschreibung und Aufstellung bestandesindividueller Ertragstafeln mit Hilfe von Wachstumsmultiplikatoren." ["Increment prognoses, projection of stand volume and stand-specific yield tables on the basis of growth multipliers.]. *Wissenschaftliche Zeitschrift der Technischen Universität Dresden* 21: 1247–1249.
- White, J. C., M. A. Wulder, A. Varhola, M. Vastaranta, N. C. Coops, B. D. Cook, D. Pitt, and M. Woods. 2013. "A Best Practices Guide for Generating Forest Inventory Attributes from Airborne Laser Scanning Data Using an Area-based Approach." *The Forestry Chronicle* 89 (6): 722–723. doi:10.5558/tfc2013-132.
- Wu, H., P. J. H. Sharpe, J. Walker, and L. K. Penridge. 1985. "Ecological Field Theory: A Spatial Analysis of Resource Interference among Plants." *Ecological Modelling* 29 (1–4): 215–243. doi:10.1016/0304-3800(85)90054-7.
- Xiao, W., A. Zafaremska, M. Smigaj, Y. Wang, and R. Gaulton. 2019. "Mean Shift Segmentation Assessment for Individual Forest Tree Delineation from Airborne Lidar Data." *Remote Sensing* 11 (11): 1263. doi:10.3390/rs11111263.
- Yao, W., P. Krzystek, and M. Heurich. 2013. "Enhanced Detection of 3D Individual Trees in Forested Areas Using Airborne Full-waveform LiDAR Data by Combining Normalized Cuts with Spatial Density Clustering." *ISPRS Annals of the Photogrammetry, Remote Sensing and Spatial Information Sciences* 2: 349–354. doi:10.5194/isprsannals-II-5-W2-349-2013.
- Zhang, Z., L. Cao, C. Mulverhill, H. Liu, Y. Pang, and Z. Li. 2019. "Prediction of Diameter Distributions with Multimodal Models Using LiDAR Data in Subtropical Planted Forests." *Forests* 10 (2): 125. doi:10.3390/f10020125.